Review

Pediatric Neurosurgery

Pediatr Neurosurg 2009;45:161–174
DOI: 10.1159/000218198

Received: May 19, 2008
Accepted after revision: September 23, 2008
Published online: May 14, 2009

The Physics of Hydrocephalus

Richard D. Penn[a] Andreas Linninger[b]

[a]Department of Surgery, University of Chicago and [b]Department of Bioengineering, University of Illinois at Chicago, Chicago, Ill., USA

Key Words
Intracranial dynamics · Hydrocephalus, unilateral · CSF flow · Brain pressure gradients · Brain pulsations

Abstract
This article reviews our previous work on the dynamics of the intracranial cavity and presents new clinically relevant results about hydrocephalus that can be gained from this approach. Simulations based on fluid dynamics and poroelasticity theory are used to predict CSF flow, pressures and brain tissue movement in normal subjects. Communicating hydrocephalus is created in the model by decreasing CSF absorption. The predictions are shown to reflect dynamics demonstrated by structural MRI and cine-MRI studies of normal subjects and hydrocephalus patients. The simulations are then used to explain unilateral hydrocephalus and how hydrocephalus could occur without CSF pulsations. The simulations also predict the known pressure/volume relationships seen on bolus infusions of CSF, and the small transmural pressure gradients observed in animal experiments and in patients with hydrocephalus. The complications and poor performance of shunts based on pressure-sensitive valves are explained and a system of feedback control is suggested as a solution.

Introduction

In their classic paper on normal-pressure hydrocephalus in 1976, Hakim et al. [1] began by noting the need for a sound, mechanical model to describe the intracranial liquid tissue complex and emphasized the importance of such a model for understanding hydrocephalus, as well as trauma, tumors, and cerebrovascular accidents. Their approach is an excellent example of how basic physical laws can provide explanations for what appear to be perplexing clinical phenomena. Similar in intent, the goal of our work has been to adopt the basic laws of physics and apply them to explain the dynamic phenomena in the intracranial cavity. In doing so, we take advantage of new computer-based mathematical techniques, MRI studies, and pressure monitoring which were not available 30 years ago. Much of our experimental work has been presented in engineering and imaging literature [2–4]. Since the goal is to advance understanding and improve neurosurgical treatments for brain diseases and in particular hydrocephalus, this review article is designed to present in a clear, relatively nontechnical manner our main findings leading to a comprehensive quantitative picture of intracranial dynamics and their implications for clinical practice.

KARGER

Fax +41 61 306 12 34
E-Mail karger@karger.ch
www.karger.com

1016–2291/09/0453–0161$26.00/0

Accessible online at:
www.karger.com/pne

Richard Penn, MD
University of Chicago, Section of Neurosurgery
5841 S. Maryland Ave., MC3026
Chicago, IL 60637 (USA)
Tel. +1 773 702 5272, Fax +1 773 702 3518, E-Mail rpenn@surgery.bsd.uchicago.edu

Hakim's Premise of the Brain as a 'Sponge'

The critical starting point in the work of Hakim et al. [1] was considering the brain parenchyma as 'an open-cell sponge made of viscoelastic material'. The volume of the brain is seen as dependent on its hydration and the state of hydration in turn is based on the external forces acting on the brain. The extracellular space, 15–20% of the brain volume, plus the brain blood volume, less than 3%, is subject to changing compressive forces. With high CSF pressure against the ventricular surface, fluid is wrung out of the parenchyma and the brain tissue deforms, particularly at the soft ependymal surface. This deformation can only occur if fluid can drain out of the brain and fluid motion, in turn, requires the existence of a pressure gradient. In contrast, venous outflow obstruction causes an equal pressure increase throughout the brain and does not cause ventricular enlargement. This key insight of the brain tissue as a deformable sponge is amply confirmed by neurosurgical observations and experimental studies. Dehydration agents such as mannitol rapidly reduce the size of the brain. The reduction of the brain size can be observed by imaging, and as the brain is shrinking, the CT density of the tissue increases indicating lower water content [5]. Inversely, an increase in extracellular fluid causes mass effect and a decrease in the tissue density. Quantitative CT and MRI imaging studies on acute hydrocephalus demonstrate large reductions in parenchymal size as the ventricles enlarge, and these changes can often be reversed with shunting [6, 7]. Measurement of brain water shows that with the restoration of the brain to its normal size with shunting, hydration in the compressed areas around the periventricular region returns to normal [6]. This is not to be confused with the disruption of the corners of the ventricular horns by stretch as hydrocephalus develops, seen as areas of hypodensity on CT. Increased intraventricular pressure has two effects as it deforms brain tissue; the ependymal surface is damaged and in the more protected, deeper regions compression decreases hydration. Removing excess CSF from the ventricles by shunting reverses both of these effects.

As Hakim et al. [1] correctly argued, reduction of the size of the brain parenchyma requires fluid drainage out of the brain and for fluid to flow a pressure gradient must exist. The sponge-like brain distributes this pressure gradient as it is deformed, and Hakim et al. predicted that in communicating hydrocephalus a large pressure gradient would be present between the ventricular surface and the outer brain surface. To explain the basis of 'normal-pressure hydrocephalus', they hypothesized that this gradient would be maintained even after the pressure becomes reduced. The maintenance of such a gradient with normal intraventricular pressure is, according to his view, due to the large size of the ventricular surface and the bioplastic changes in the brain tissue that redistribute the pressure gradient. Water cannot shift back to the 'over-squeezed and distorted parenchymal sponge' [1, p. 204].

The problem with the explanation of Hakim et al. of the dynamics of hydrocephalus is that the large pressure differences they predicted are not found in humans with hydrocephalus or in animals with experimentally induced hydrocephalus [8]. An example from our animal studies is shown in figure 1. The pressures in the subarachnoid space, brain parenchyma, and ventricles were measured both acutely and chronically before, during, and after hydrocephalus was induced by a kaolin injection. Using implanted monitors that could measure the absolute pressure and the pulse pressures to ± 0.5 mm Hg no pressure differences were detected at any time during the initial evolution of hydrocephalus, at the peak of the process, nor at the 'normal' pressure period when the large ventricles still exist. Small differences in pressure of less than the 1.0 mm Hg could have been missed, but large pressure differences posited by Hakim et al. were not seen. The human data is more difficult to obtain but clearly points in the same direction; large pressure differences are not observed in communicating hydrocephalus [8–10].

How can this basic mismatch of the theory of Hakim et al. and experimental facts be explained? From the purely fluid dynamic standpoint, the brain's extracellular space, the subarachnoid space and the ventricular fluid are connected, so large pressure differences would induce massive fluid motion. If there were a sizable pressure gradient, fluid would move until the gradients were dissipated. In the static situation, without fluid movement, there can be no gradients. The situation is however not static. CSF flows through the ventricular system to the subarachnoid space with each cardiac pulsation. About one third of the CSF is produced in the brain and goes into the ventricles. To understand what is happening when hydrocephalus develops, it is necessary to consider these dynamic aspects of CSF in normal subjects and then what happens when CSF absorption is impaired as in hydrocephalus. A number of authors have stated the case for just such an approach and have marshaled the clinical reasons and experimental evidence for paying attention to the altered dynamics of fluid motion in hydrocephalus [11, 12]. An electrical analogy has been suggest-

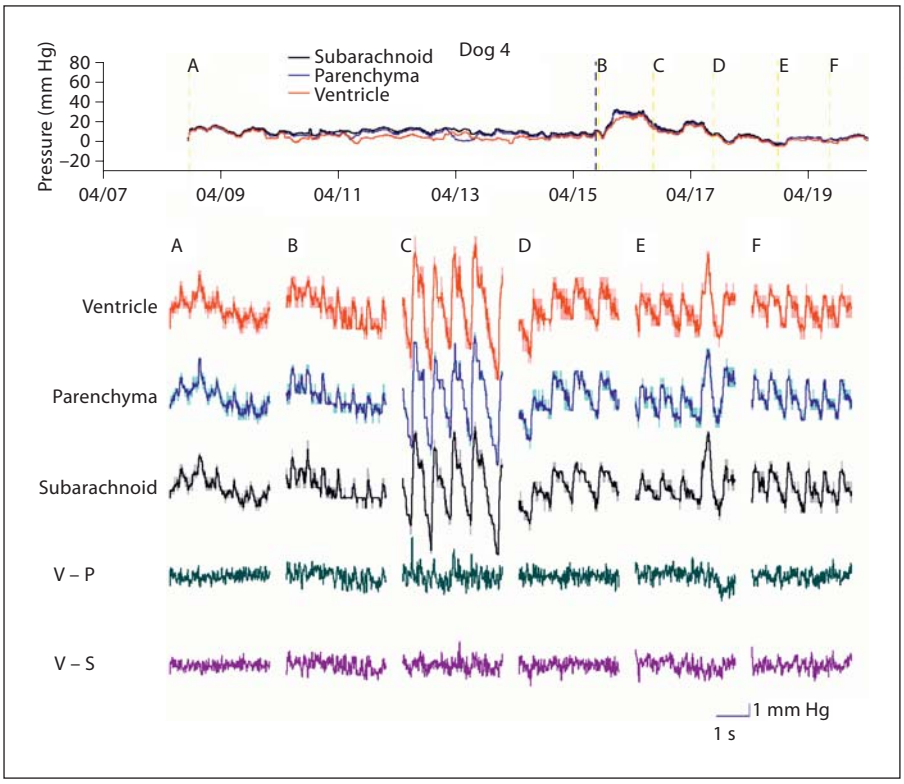

Color version available online

Fig. 1. Dog experiments showing the same ICP in subarachnoid space (S), parenchyma (P) and ventricles (V). This is true before hydrocephalus was induced by kaolin injection (lanes A and B), during development (lanes C and D), and the later normal pressure period (lanes E and F) [modified from 8].

ed as of a model to explain fluid dynamics in hydrocephalus [13]. Unfortunately, this electrical model is unsuccessful in predicting the large changes in ventricular size which occur. We have taken a different approach and applied fluid dynamic principles to the problems; then we have checked our prediction with MRI flow measurements in normal subjects and in hydrocephalic patients. The model has been built from simple to complex, step by step. For example, the original model had the CSF pulsations driven by the arterial pulse of the choroid plexus. When our measurements of ventricular wall movement showed that the ventricle size decreased with the arterial pulse we modified the model by incorporating the blood influx into the brain tissue. The model then correctly represented the timing of the brain tissue expansion and the decreased size of the ventricles. Likewise, including the spinal subarachnoid space was necessary to explain prepontine fluid movements accurately. Our current model provides a physics-based explanation for hydrocephalus which has been validated by MRI studies and which also resolves the problems with Hakim's pressure gradient hypothesis. For the interested reader, the detailed assumptions and the mathematical approaches are described in several of our recent articles in engineering journals [2–4].

Movement of CSF

The movement of CSF has two components, the net steady flow from the ventricles to the subarachnoid spaces and finally to its sites of absorption over the convexities of the brain and the pulsatile flow superimposed upon this movement. Measurements of CSF through the aqueduct of Sylvius indicate that the cyclic in and out flow is about 5 times higher than the net flow out of the ventricular system [14, 15]. Therefore, the kinetic energy of flow is much higher for the pulsations than the steady forward flow. The driving force for the net flow is the production of CSF at the normal rate of about 0.3 ml/min, or a turnover rate of 4 or 5 times per day. CSF production in turn is due to the arterial pressure and active and passive transport in the choroid plexuses and the brain tissue. Ventricular perfusion studies suggest that as much as a third of CSF coming from the ventricles is produced by the brain, and diffusion experiments demonstrate a flow of extracellular fluid from the deep brain parenchyma toward the ventricular surfaces [16–18].

The pulsatile movement of CSF is due to the expansion of the cerebral vasculature with each cardiac cycle. The brain gets 20% of the cardiac output, and as the blood flows into the intracranial arteries they expand. As the

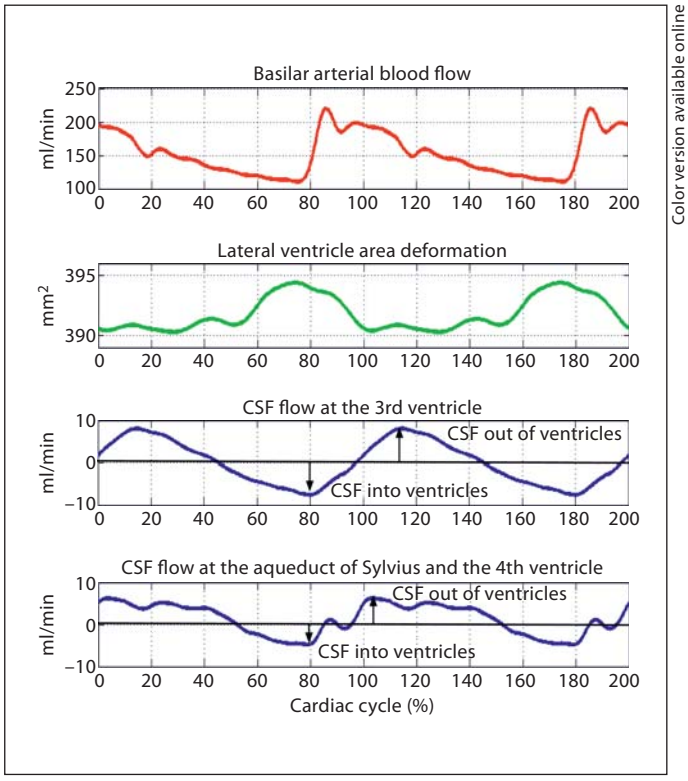

Fig. 2. Cine-MRI measurements of the blood flow in the basilar artery, the lateral ventricle area deformation, the CSF flow at the 3rd ventricle, and at the junction of the aqueduct of Sylvius and the 4th ventricle for a normal subject for two cardiac cycles. Note that the basilar artery pulse comes first, the ventricle then starts to become smaller and finally CSF goes out into the subarachnoid space [modified from 4].

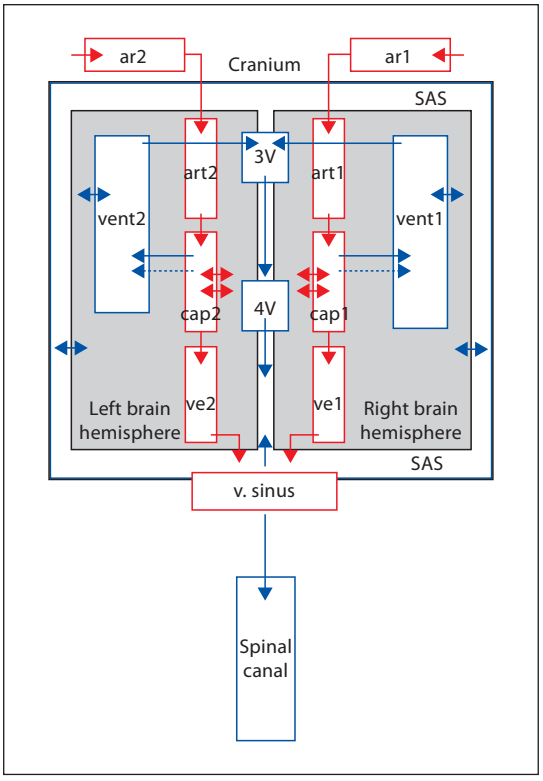

Fig. 3. The main blood compartments are the arteries (ar), arterioles (art), capillaries (cap), veins (ve), and venous sinus (v. sinus). The CSF system is composed of the lateral ventricles (vent), third and fourth ventricles (3V, 4V), subarachnoid space (SAS) and the spinal canal (outside of the cranium). The parenchyma is divided into the right and left hemisphere.

impulse continues into the small arterioles and capillary system in the brain parenchyma, it expands these vessels in the brain tissue. This expansion forces CSF out of the ventricular system and the cerebral subarachnoid spaces, and the CSF moves into the more compliant spinal subarachnoid space. CSF has to be displaced outside the almost rigid cranial cavity because blood, CSF and brain tissue are mainly incompressible water. The pattern reverses in diastole. This flow pattern can be seen and accurately quantitated by cine-MRI studies timed to the cardiac pulsations [4]. In figure 2 from our MRI studies on normal subjects, the bolus of blood in the basilar artery is measured as well as the movement of the ventricular wall inward as the brain expands and the flow of CSF out of the lateral and third ventricles. Note that, as expected, the bolus of blood arrives before the ventricles contract and pushes CSF out of the ventricular system into the spinal subarachnoid space.

Using appropriate equations governing fluid movement and the sizes of the fluid spaces, these motions can be precisely computed [2, 3]. The scheme for representing this is shown in figure 3 and the relevant equations and constants from the literature are listed in table 1. The computations can be simplified with reasonable accuracy to two dimensions corresponding to the sagittal cine-MRI, and the measured and computer-generated results can be compared. Figure 4a shows that the predictions of velocity match the velocity seen in the cine-MRI. Thus, using a simple forcing function representing the carotid pressure wave entering the intracranial cavity and knowing the sizes of the fluid spaces, the appropriate laws of physics predict the induced fluid pulsations. The cerebral vasculature expansion is about 1–2 cm^3 and this drives fluid in and out of the ventricles. Knowing the fluid flow makes it possible to derive the pressure gradient driving this flow. The results are also illustrated in figure 5a. Note

Table 1. First principle equations and constants used in the model

Continuity for blood	$\frac{\partial A_b}{\partial t} + \vec{\nabla} \cdot \left(A_b \vec{u}_b\right) = 0$	(1)
Momentum for blood	$\rho_b \left(\frac{\partial \vec{u}_b}{\partial t} + \vec{u}_b \cdot \vec{\nabla} \vec{u}_b \right) = - \vec{\nabla} p_b + \mu_b \vec{\nabla}^2 \vec{u}_b$	(2)
Distensibility of vessel wall	$m \frac{\partial^2 A_b}{\partial t^2} + k_b \frac{\partial A_b}{\partial t} = E_b f\left(A_b, A_{0_b}\right) - \Delta p_b$	(3)
Continuity for the extracellular fluid	$\frac{\partial \zeta}{\partial t} = - \vec{\nabla} \cdot \vec{q}$	(4)
Darcy's law for the extracellular fluid	$- \vec{\nabla} p = \frac{\mu}{k} \vec{q} \Rightarrow \frac{\partial \zeta}{\partial t} = \frac{k}{\mu} \vec{\nabla}^2 p$	(5)
Change in the extracellular fluid content ζ	$\zeta = \frac{\partial \phi}{\partial t}$	(6)
Force balance for the solid phase of the biphasic poroelastic medium	$\rho_s \frac{\partial^2 \vec{d}}{\partial t^2} = G \vec{\nabla}^2 \vec{d} + \frac{G}{1-2\nu} \vec{\nabla} \varepsilon - \alpha \vec{\nabla} p$ $\varepsilon = \vec{\nabla} \cdot \vec{d}$ and $\dot{\vec{d}} = \vec{u}_s$	(7)

Location	Elastance, Pa	Volume, cm^3
Arteries, ar	27.3×10^4 [34]	30.0 [34]
Arterioles, art	40.0×10^4 [34]	16.0 [34]
Capillaries, cap	44.0×10^4 [34]	20.0 [34]
Venules, ven	117.0×10^4 [34]	70–80 [34]
Veins, ve	$(5.0–27.3) \times 10^4$ [34]	
Venous sinus, v. sinus	2.6×10^4 [34]	13 [34]
Ventricles, vent	N/A	15–20 [3, 35]
Cerebral SAS, SAS	N/A	30 [36]
Spinal SAS, sp. canal	1.0×10^6 [37, 38]	90–100 [36]
Brain parenchyma	$(1.0–10.0) \times 10^3$ [39, 40]	1,400 [36]

$\vec{u}_b \mu_b$ = Velocity vector, viscosity; A_b = cross-sectional area; $p_b \rho_b$ = blood pressure, density; m = mass of the membrane; k_b = dissipative dampening coefficient; E_b = Young's modulus; A_{0_b} = cross-sectional area; $\vec{q}$ = Darcy velocity; p = pressure outside the vessel walls; ε = volumetric strain; $\vec{d}$ = displacement vector of solid matrix; $G\nu$ = shear Young's modulus, Poisson ratio; ρ_s = density of the biphasic medium; ζ,ϕ = fluid content, porosity change.

that at no point in time during the cycle is the pressure gradient between the ventricles and the subarachnoid space more than plus or minus 0.6 mm Hg.

The same computer-generated analysis of CSF flow can be performed for hydrocephalic patients. The relevant sizes of the CSF spaces and flow are taken by T_1 and cine-MRI measurements. Figure 4b shows the actual flow at the aqueduct for a patient with communicating hydrocephalus and the predicted flow. The cine-MRI flow is similar to that predicted by the physics and that flow is 3 times faster than in normal subjects. This increased flow is consistent with the findings of other cine-MRI studies [14]. In fact, increased CSF flow through the aqueduct has been suggested as a good marker for hydrocephalus since it is not seen with cerebral atrophy [19, 20].

Knowledge of flow rates again allows the calculation of pressure gradients producing the cyclic flow. The results comparing the normal subjects and hydrocephalic patients are seen in figure 5. The gradient between the subarachnoid space and the ventricles is almost identical between them and is below the 1 mm Hg sensitivity of the intracranial pressure (ICP) monitors. The cine-MRI

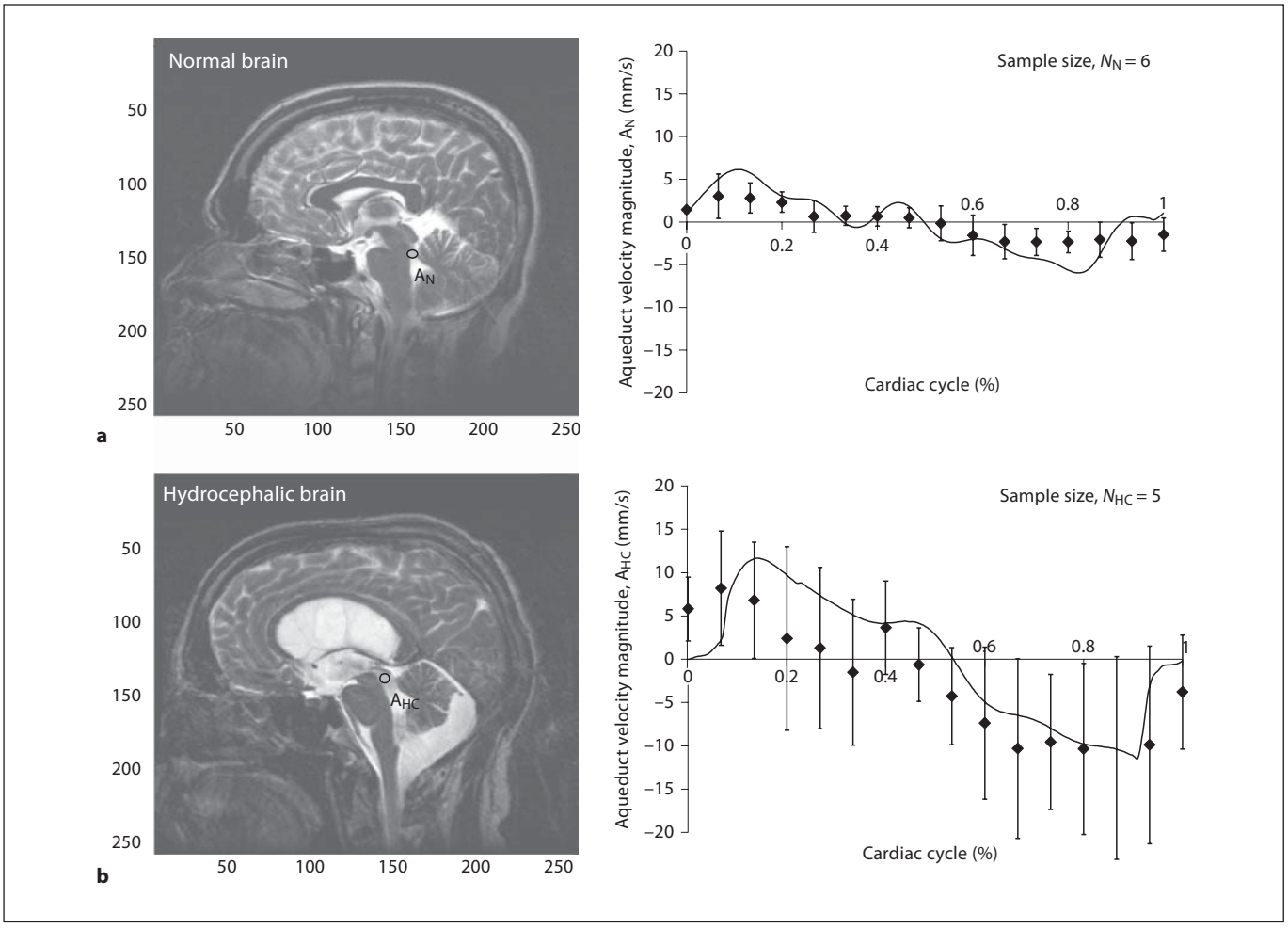

Fig. 4. a In normal subjects the average peak velocity at the aqueduct of Sylvius was found to be 7 mm/s. The velocity measurements are based on 6 normals. The computer predictions are shown in solid lines. **b** In the hydrocephalic case, the amplitude is on the average over 3 times higher with the peak velocity 23 mm/s. The velocity measurements are based on 5 hydrocephalic subjects. The computer predictions are shown in solid lines.

studies in hydrocephalus are consistent with clinical and animal pressure measurements. They once again raise the question of how such pressure gradients could create hydrocephalus and how to modify the analysis of Hakim et al. of what is happening in brain tissue.

The Brain Parenchyma

The central clinical concern of hydrocephalus is not with the abnormal size of the ventricles but the deformity of the brain tissue and its consequences. Studies of the pathological effects of hydrocephalus clearly demonstrate progressive damage to the ependymal surface and periventricular areas [21]. These regions are the most stretched and deformed, and the blood vessels are elongated and compressed, resulting in ischemia. The tissue away from the ventricular surfaces can be compressed by displacing extracellular fluid and is, at least initially, spared from neuropathological changes. The often remarkable restoration of brain tissue size after shunting reflects these reversible compressive properties of the brain tissues. To understand the physical properties of brain tissue, the physics of a fluid-filled matrix must be applied. The situation is complex because the brain consists of an interconnected cellular matrix and the extracellular space with its maze-like connectivity, as well the brain's vascular system. In itself, this is a daunting problem, but added

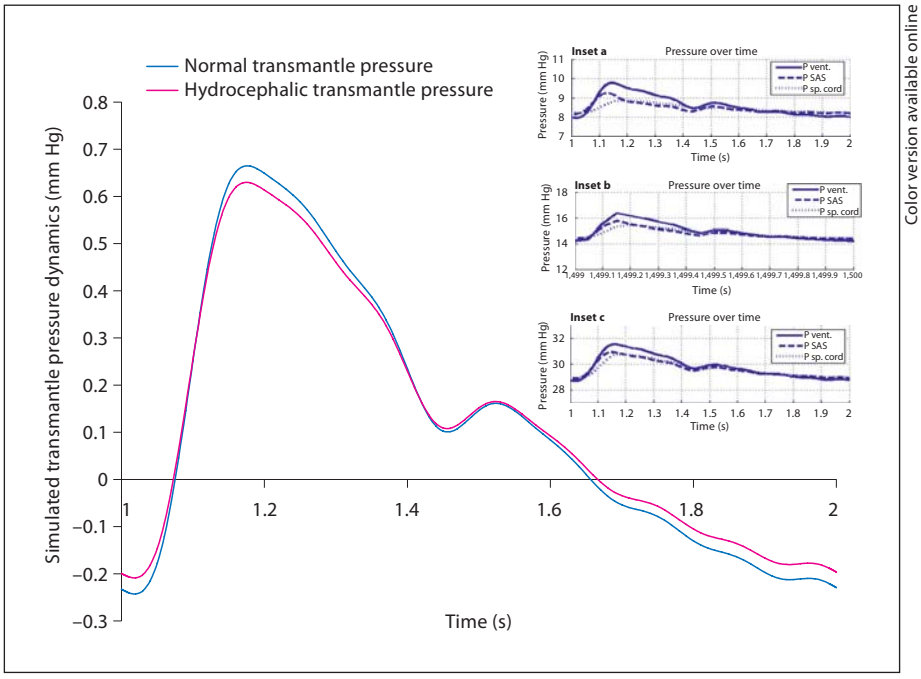

Color version available online

Fig. 5. Intracranial pressure signals in normal conditions (inset a), transient phase (inset b) and fully developed communicating hydrocephalus (inset c). The simulations confirm that only small transmantle pressure differences occur in communicating hydrocephalus. Moreover, in each cardiac cycle, there is a pressure sign change, indicating a pulsating loading pattern of the parenchyma. P vent. = Pressure ventricle; P SAS = pressure subarachnoid space; P sp. cord = pressure spinal cord.

on are the problems of quantitatively describing how CSF in the ventricles interacts dynamically with the brain tissue as the ventricles expand. Needless to say, we have not solved all of these problems. However, we can now suggest an approach that taken step-by-step can provide insight into the physics of hydrocephalus. The physics in turn reveals why our shunting systems have such a high failure rate.

To apply physical analysis to the matrix fluid, the laws governing such dual symptoms formulated by Biot [22] need to be applied. They deal with how forces produce fluid flow through the spaces between the matrix and how the matrix is deformed as the fluid moves. Fortunately, a great deal is known about the brain's extracellular space, its dimensions and tortuosity, and how substances diffuse through it. Likewise, many of the important physical characteristics of brain tissue have been measured, so reasonable approximations of the tissue's compressibility are available. To use this information in a realistic, three-dimensional representation of the brain, modern tools of imaging and computer science can be employed.

The steps in the analysis are shown in figure 6. A high-quality MRI of a subject displaying the relevant brain anatomy (white matter, gray matter, ventricular spaces) is obtained. Reconstruction tools are applied, and the image is then broken up into a grid. The grid points are con-

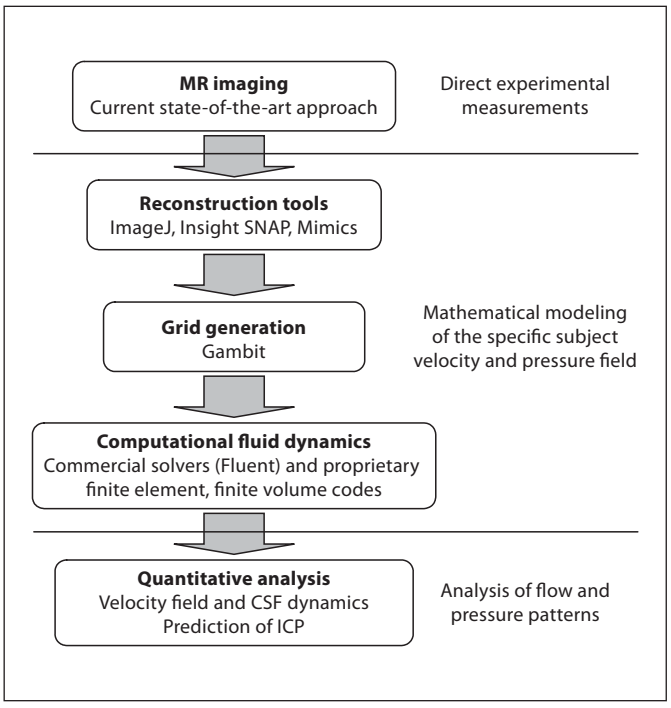

Fig. 6. Schematic of the computer steps used.

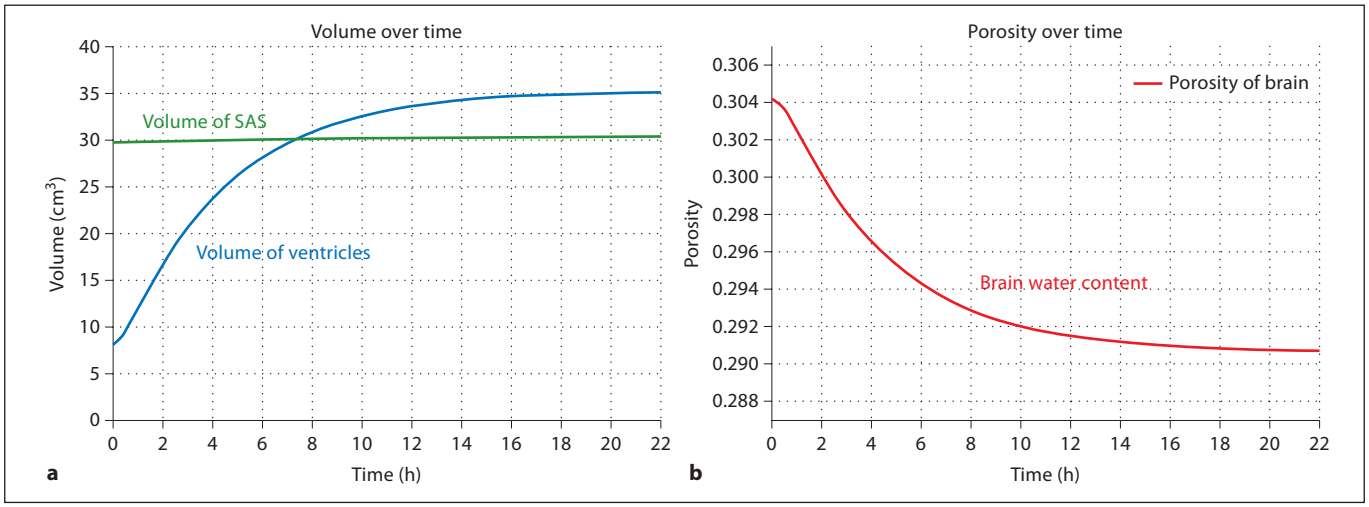

Fig. 7. Simulated communicating hydrocephalus. **a** Volume increase in the ventricular system and cerebral subarachnoid space after a reabsorption block, communicating hydrocephalus. **b** Change in porosity of the brain parenchyma as communicating hydrocephalus develops. SAS = Subarachnoid space.

nected to make up the surfaces of the structures and then placed into a computational space called a finite volume model. This defines adjacent points that make up the volume and the relationships the volumes have to their neighbors. The relationships of these volumes are then defined by the equations that describe the matrix and fluid interactions. It is at this point that the fluid dynamic laws applicable to the brain's fluid/solid matrix are inserted into the system.

As already discussed, we have developed an accurate description of the CSF fluid flow within the CSF spaces for both normal subjects and patients with hydrocephalus. This information is used to estimate the forces which press against the brain tissue with normal absorption of CSF and when absorption becomes obstructed with hydrocephalus.

The next step is to describe what happens to the brain tissue. When absorption decreases, fluid accumulates within the expandable ventricular system, and the stretched parenchyma surface resists, raising the ICP. Up to this point, events are intuitively obvious. However, as the ventricular size enlarges and brain tissue is displaced and fluid moves within the brain's fluid/solid matrix, a finite volume model is necessary to provide an explanation of the changes. For validation the predictions from the model can be compared to the changes seen on imaging. If they correspond then it is reasonable to conclude that the way the physical laws have been applied is correct and the laws of motion in porous media provide insight into the complex behavior of the brain tissue. Both the slowly increasing accumulation of CSF due to a decrease in CSF absorption and the second-to-second pulsations of the vascular system, brain and CSF spaces can be included in the simulations. In this way, the fast dynamic as well as the slow changes can be predicted.

Figure 7 shows the ventricular enlargement which is predicted as CSF absorption is decreased by 90%. The ventricles become rounded at the points of greatest curvature, and then they expand relatively uniformly. As this continues, fluid flow reverses and goes into the brain parenchyma where it is absorbed. The brain parenchyma away from the ventricular surface is compressed, producing a decrease in brain size. As the brain gets smaller, the brain water decreases (fig. 7b).

In addition to the brain fluid/matrix, the blood in the brain parenchyma needs to be considered. It is the source of the CSF formation in the brain and in the hydrocephalic state the likely sink of fluid removal. The blood vessels in the intracranial cavity can be represented by a network of connected distensible tubes. The size of the arteries, arterioles, capillaries, and veins has been accurately measured in previous anatomical studies, and this allows prediction of flow patterns based on the known driving force from the heart. The predicted velocities and pressures are consistent with known physiological measurements. For example, the pressure falls dramatically in the capillaries, but significant pulsations in flow are still seen (fig. 8).

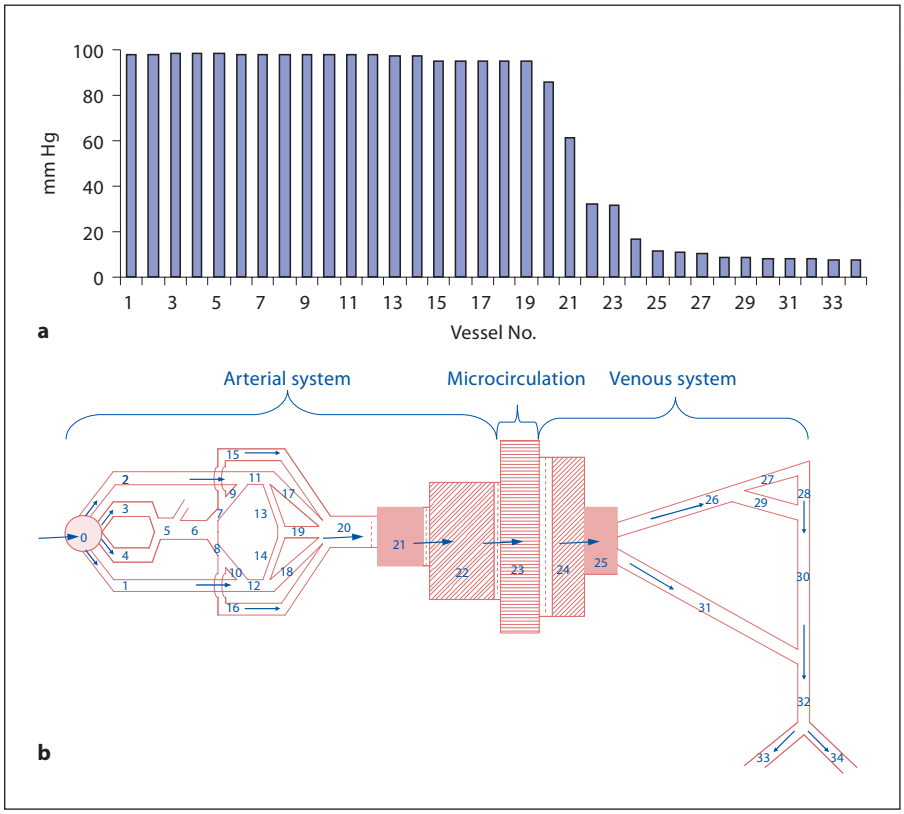

Fig. 8. a Mean pressures in the cerebral vasculature. The compartment indices are according to the schematic shown in **b**.

It is possible to place this system of vessels and their blood flow into the computer-generated representation of the brain parenchyma. Arteries and the larger arterioles as well as the larger veins are outside of the brain parenchyma. The elastic properties of arteries produce CSF displacement in the subarachnoid space with each pulsation. More importantly, the parenchyma is displaced by the bolus of blood as it goes into the small arterioles and the capillary system. The displacements due to capillary bed filling within the fluid/matrix of the brain can then be predicted. Enlargement of the brain is approximately 2 cm^3 and this is divided between the ventricles getting smaller and the cortical surface pushing outward. The amount of CSF displaced out of and then back into the ventricular system with each cardiac cycle is a little less than 1 cm^3. The other approximately 1 cm^3 of increased blood volume in the brain is presumed to displace the brain outward, but is too small to be accurately measured by MRI. This same type of calculation can also be done for the hydrocephalic state. In this case the model predicts that the CSF pulse pressure and the amount of fluid moving are increased. This key finding is confirmed by cine-MRIs of patients with hydrocephalus [12, 23].

The stretching of the capillaries in the white matter around the ventricles is represented by movements of the points on the grid surface as hydrocephalus develops. The combination of the stretching, the increased ICP, and the consequent decrease of flow leads to ischemic changes in the periventricular region. However, our current model does not yet have enough spatial resolution to predict when ischemia will occur. How much the vessels can be stretched and still maintain flow is not known. Potentially, MRI perfusion studies of cerebral blood flow will provide such information. At present, the simulation only allows the reasonable conjecture that the flow will decrease and ischemic changes will occur where the stretching is greatest, that is in the periventricular white matter.

Clinical Implications

Several important clinically relevant deductions can be reached from this analysis. First of all, large pressure differences are not needed to cause communicating hydrocephalus. Small gradients in pressure can slowly en-

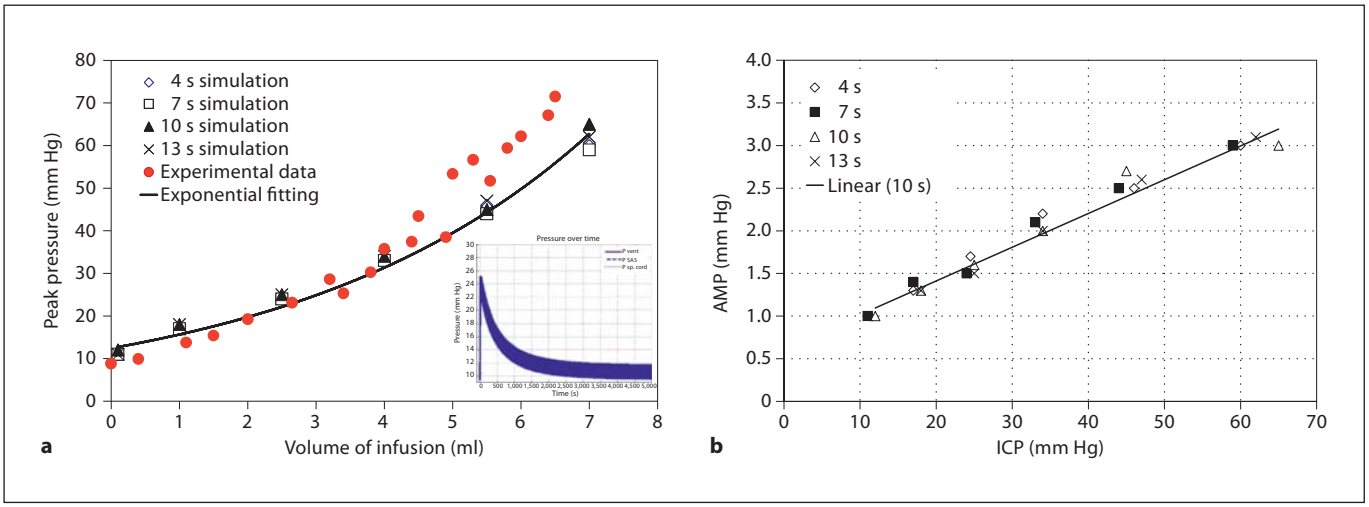

Fig. 9. Experimental results of bolus injections in humans versus simulated results from the model. **a** Peak pressure – volume of infusion (P – V) for short infusion times. Infusion times 4, 7, 10 and 13 s. In the zoomed window on the right lower side the ventricular ICP trajectories after bolus injection in the subarachnoid space are shown. After 1.4 h the pressure returns to normal level. **b** Simulated relationship between pulse amplitude (AMP) and mean ICP for four different infusion times.

large the ventricles with little ICP elevation. This conclusion was reached by Levine [24] in his analytical solution to Biot's equations, and that same behavior is seen in our simulations using MRI-demonstrated anatomy. A high ICP can occur when the buildup of CSF is rapid, but as equilibrium is reached and fluid is removed by absorption into the capillary system the ICP can go back to normal. Like soil which has been subjected to a pressure gradient and loses fluid, the brain does not return to its initial volume unless fluid flows back into it.

A related point is that the ICP is not the best indicator of compression of the brain. A compressed brain will have a different compliance because dynamic loading of the tissue causes stretching of some regions and compression of others. This change in the matrix will be reflected in a higher than normal pulse pressure, regardless of the ICP. Acutely, pulse pressure goes up as ICP increases, but once the tissue changes, the ICP will decrease and not be a reliable indicator of the compressed state of the brain tissue. The pulse pressure due to the volume of the blood injected into the intracranial cavity will, in contrast, reflect brain compliance. Patients with cerebral atrophy have normal or low pulse pressures and patients with normal pressure hydrocephalus have high pulse pressures [23]. Acute infusion tests also reflect this, since high R_o values reflect a compressed, less-compliant system, as well as increased output resistance [25].

The physical model of brain dynamics can be used to explain the results of CSF infusion tests. The pressure volume relationship when a fluid bolus is placed in the spinal subarachnoid space can be predicted (fig. 9). In the model, as the volume of injected fluid increases, the ICP increases producing a pressure volume curve which is similar to that seen in patients. Most of the effect is due to the elasticity of the spinal subarachnoid space, and a small proportion is due to brain stiffness and venous compression. The CSF pulse pressure increases as ICP goes up due to the decreasing compliance of the whole dynamic system.

The physical principles also predict the occurrence of unilateral hydrocephalus when the choroid plexus is removed from one lateral ventricle and an absorption block of CSF is created in the subarachnoid space. The animal experiments performed by Bering [26] and later Wilson and Bertan [27] called attention to the role of the choroid plexus pulsations in creating hydrocephalus. The interpretation of these findings has been that in some way the pulsations are basic to producing hydrocephalus because the pressure should be the same in the connected ventricles. However, careful analysis of pressure relationships between the ventricles using the model shows that only slight pressure differentials are needed to produce asymmetrical hydrocephalus.

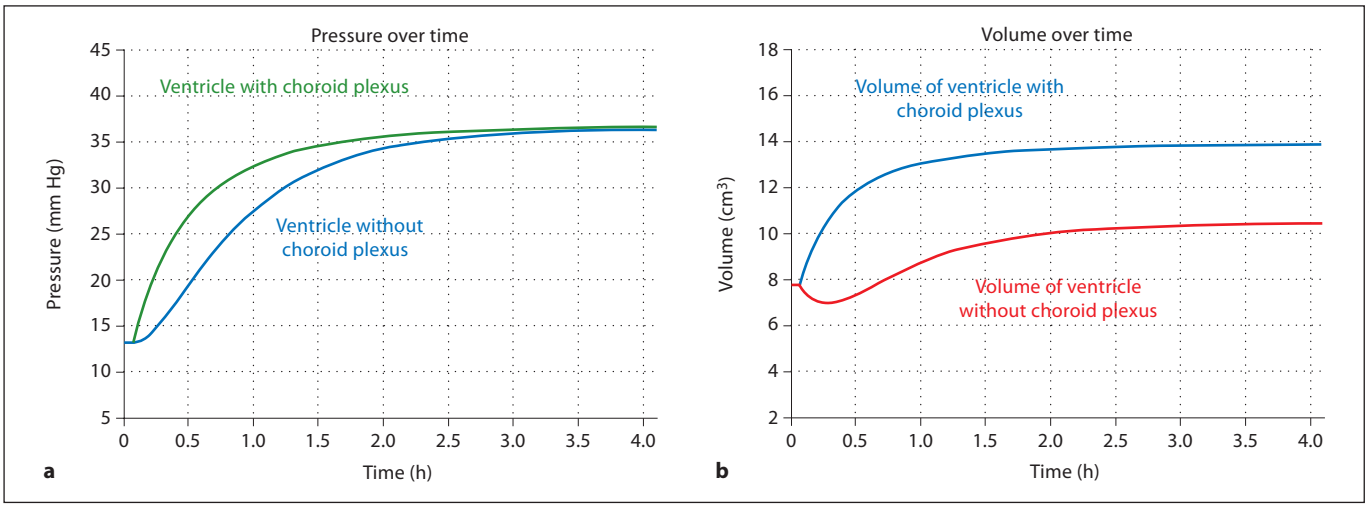

Fig. 10. Simulation of hydrocephalus when the left ventricle is plexectomized and the foramina of Monroe is open. **a** ICP rise for both lateral ventricles. **b** Volume accumulation in both lateral ventricles. Asymmetrical hydrocephalus occurs with a difference of 4.0 cm^3 between the two ventricles, as found in animal experiments.

Using the model's predictions, figure 10a shows the ICP buildup in the lateral ventricles in the case where the choroid plexus in the left lateral ventricle has been removed and both foramens of Monroe are open. Due to the lack of the choroid plexus in the left lateral ventricle, on that side there is no production of CSF and lower pulsatility leading to mean pressures which are slightly lower than the intact ventricle. As a result the model predicts that the volume expansion of the left lateral ventricle is delayed and never reaches the final volume of the right (with intact choroid plexus) lateral ventricle as shown in figure10b. The volume difference between the two lateral ventricles is approximately 4.0 cm^3. Overall, the mean pressure, pulsatility and ventricular expansion were smaller in the ventricle with no choroid plexus. The predictions are similar to the animal observations. Thus the first-principles mechanistic approach gives a plausible quantitative explanation for the development of asymmetric hydrocephalus.

A prediction can also be made of what would happen with bilateral plexectomies. One can completely stop pulsations in the model by making the arterial input nonpulsatile. If an absorption block is then simulated, ventricular enlargement still occurs at the same rate and to the same degree.

The physical dynamics in intracranial cavity which we have simulated explain quantitatively many clinical and experimental observations. (1) Communicating hydrocephalus is produced by a reabsorption problem; (2) transmural pressures are small, but essential to the expansion of the ventricular system; (3) appropriate pressure volume relationships are predicted by the simulations; (4) unilateral hydrocephalus can occur due to pulsation differences that result in slight imbalances of the pressure gradients between the ventricles; (5) hydrocephalus can occur without pulsations due to reabsorption block, and (6) normal pressure hydrocephalus can be explained by the properties of a poroelastic brain. Hysteresis is an expected property and the altered brain tissue matrix is not completely reversed by simply restoring reabsorption to normal.

While physical analysis of the dynamics of fluid flow in the intracranial cavity provides an explanation of normal pressure hydrocephalus and the deformities of tissue that take place in hydrocephalus, it does not account for the chronic biological changes which take place. In the extreme situation, hydrocephalus causes ischemia, and the tissue damage in turn changes the tissue characteristics permanently [21]. Periventricular edema changes the flow of fluid as cells are torn apart. Loss of cells and myelin also changes the matrix. What Hakim et al. referred to as 'bioplastic' changes in tissue needs to be quantified. MRI techniques which are now being developed to measure tissue elasticity and perfusion noninvasively may

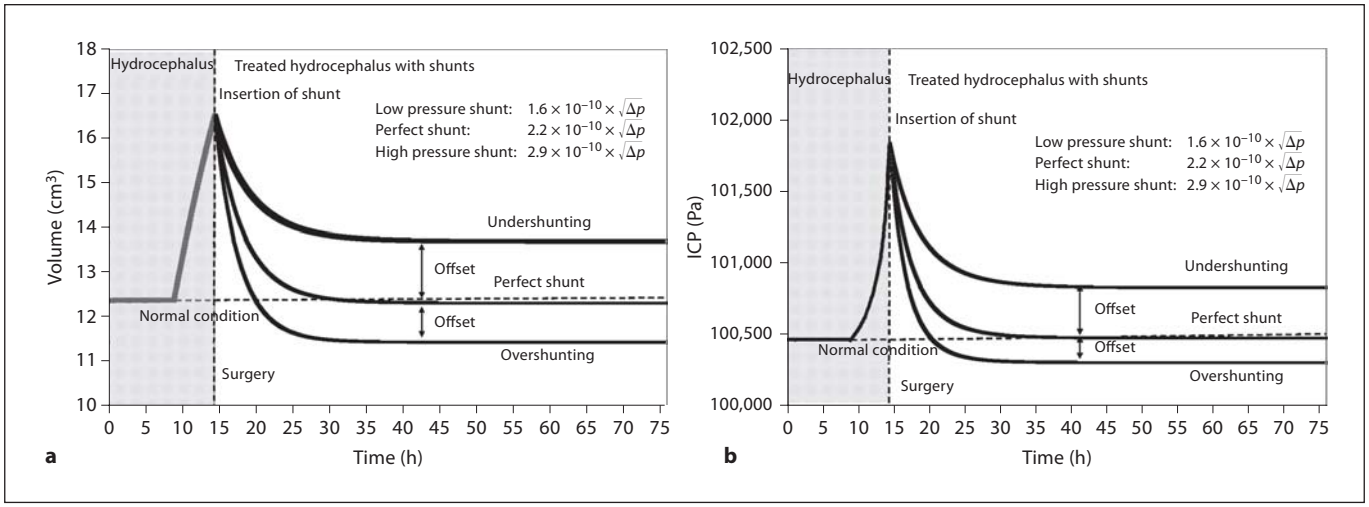

Fig. 11. Simulated change of the lateral ventricle size (**a**) and pressure (**b**) after 'shunting' with three different pressure valves. Note the effects of choosing the wrong pressure on volume and pressure (under- or overshunting).

help resolve these unknowns [28]. For the present, it means that we cannot predict precisely how the brain will respond from its compression with fluid removal. However, to reverse the compression considerable drainage via a shunt is needed to create a pressure gradient to draw back fluid into the parenchyma and then into the ventricles. If the shunt system continues to drain when the ventricles come down to normal size, the result will be overdrainage and small ventricles leading to the slit-ventricle syndrome and obstruction of the catheter. If drainage of fluid via the shunt is too small, the gradient will be insufficient to pull the brain tissue toward a more normal configuration, and recovery of the compromised vasculature will not occur. However, adjustable pressure valve systems may provide a better way to meet the varying needs. ICP is not a good guide for fluid drainage because it does not fully reflect the brain's hydration or shape.

Current shunt valve systems work by sensing ICP. They do not function as simple bench testing might suggest [29, 30]. ICP in the ventricles is negative in the standing position, positive lying down, and varies with venous pressure changes and barometric pressure changes. The flow in a shunt system can vary by a factor of 200 times during the day, from 0.01 to 1.93 mm/min [31]. The flow in the shunt valve is also complicated by the effect of pulse pressure which changes shunt resistance. These considerations alone would suggest that any shunt system based on pressure or differential pressures alone will have unpredictable nonphysiological responses to CSF dynamics. The high failure rate of shunts and the common problem of slit ventricles underscore how ill-suited our current shunting systems are.

Our new understanding of the mechanics of the brain fluid/matrix also makes it clear why our current systems may fail. Figure 11 shows how different pressure valves would be expected to reduce ventricular size and pressure, assuming linear elastic brain tissue. Only the 'perfect' valve exactly matching the absorption block would work. The change in the brain fluid matrix makes the situation even more complex because as the brain changes size the biological stiffness properties of the tissue matrix change. Knowing how to choose the right valve characteristics in a specific patient is well beyond the current knowledge we have about the brain, especially the brain already changed by hydrocephalus. It is not surprising that the available shunt systems are indistinguishable in terms of outcome [32]. There are alternatives. Hakim [33] pointed out the mismatch of shunts to physiological needs over 30 years ago and suggests a servovalve shunt.

Third ventriculostomy is an excellent procedure in some patients with proximal obstructions. Improvement in symptoms frequently occurs without significant reduction in ventricular size. This is now understandable, since it often takes large overdrainage of CSF to rehydrate the brain and decrease ventricular volume. Restoring absorption to normal in these patients does not create a big enough gradient to change the matrix size by fluid flow.

A novel engineering approach to solve the problem of overdrainage would be to monitor a variable like ventricular size and use a feedback system to control removal of CSF until the appropriate size is reached. This feedback avoids guessing what flow is necessary. The amount of flow would be governed directly by the difference between the actual size and the desired size. Other possibilities for feedback control could be pulse pressure, pO_2, tissue stress, or neural activity. The point is that feedback control is a better way to arrive at a desired outcome than trying to guess what might work with simple or complex pressure valves. Such guessing will not work reliably in a complex system in which many tissue characteristics cannot yet be measured and may change over time.

Our model needs to be extended to the special conditions of pediatric hydrocephalus. The boundary condition of a fixed cranial size must be modified and the effect of an open fontanelle included. Furthermore, the infant brain has a higher water content so the tissue compliance and fluid movement may be very different from the adult brain. Likewise, the ageing brain may have important differences in tissue characteristics and different elasticities. Clearly there is much work to be done in modeling these situations. The results of the current model encourage such extensions of this approach. Basic laws of physics, appropriately applied to the complex physiology of hydrocephalus, have already provided insight into the mechanics of hydrocephalus. The clinical challenge is to use our understanding to produce shunting systems that can deal with the altered brain physiology and result in better outcomes for our patients.

Acknowledgments

The study was funded by the Brainchild Foundation (R.D.P.), STARS Kids Foundation (A.L.), Susman-Asher Foundation (R.D.P.), and Medtronic Inc. (R.P.).

References

1 Hakim S, Venegas JG, Burton JD: The physics of the cranial cavity, hydrocephalus and normal pressure hydrocephalus: mechanical interpretation and mathematical model. Surg Neurol 1976;5:187–210.
2 Linninger AA, Tsakiris C, Zhu DC, Xenos M, Roycewicz P, Danziger Z, Penn R: Pulsatile cerebrospinal fluid dynamics in the human brain. IEEE Trans Biomed Eng 2005;52:557–565.
3 Linninger AA, Xenos M, Zhu DC, Somayaji MR, Kondapalli S, Penn RD: Cerebrospinal fluid flow in the normal and hydrocephalic human brain. IEEE Trans Biomed Eng 2007;54:291–302.
4 Zhu DC, Xenos M, Linninger AA, Penn RD: Dynamics of lateral ventricle and cerebrospinal fluid in normal and hydrocephalic brains. J Magn Reson Imaging 2006;24:756–770.
5 Meining G, Aulich A, Wende S, Reulen S: The effect of dexamethasone and diuretics on peritumor brain edema: comparative study of tissue water content and CT; in Pappius H, Feindel W (eds): Dynamics of Brain Edema. New York, Springer, 1976, pp 300–305.
6 Penn RD, Bacus JW: The brain as a sponge: a computed tomographic look at Hakim's hypothesis. Neurosurgery 1984;14:670–675.
7 Penn RD, Belanger MG, Yasnoff WA: Ventricular volume in man computed from CAT scans. Ann Neurol 1978;3:216–223.
8 Penn RD, Lee MC, Linninger AA, Miesel K, Lu SN, Stylos L: Pressure gradients in the brain in an experimental model of hydrocephalus. J Neurosurg 2005;102:1069–1075.
9 Stephensen H, Tisell M, Wikkelso C: There is no transmantle pressure gradient in communicating or noncommunicating hydrocephalus. Neurosurgery 2002;50:763–773.
10 Czosnyka M, Pickard JD: Monitoring and interpretation of intracranial pressure. J Neurol Neurosurg Psychiatry 2004;75:813–821.
11 Greitz D, Greitz T: The pathogenesis and hemodynamics of hydrocephalus. Int J Neuroradiol 1997;3:367–375.
12 Greitz D, Hannerz J, Rahn T, Bolander H, Ericsson A: MR imaging of cerebrospinal fluid dynamics in health and disease. On the vascular pathogenesis of communicating hydrocephalus and benign intracranial hypertension. Acta Radiol 1994;35:204–211.
13 Egnor M, Zheng L, Rosiello A, Gutman F, Davis R: A model of pulsations in communicating hydrocephalus. Pediatr Neurosurg 2002;36:281–303.
14 Greitz D: Cerebrospinal fluid circulation and associated intracranial dynamics. A radiologic investigation using MR imaging and radionuclide cisternography. Acta Radiol Suppl 1993;386:1–23.
15 Naidich TP, Altman NR, Gonzalez-Arias SM: Phase contrast cine magnetic resonance imaging: normal cerebrospinal fluid oscillation and applications to hydrocephalus. Neurosurg Clin N Am 1993;4:677–705.
16 Cserr HF, Cooper DN, Milhorat TH: Flow of cerebral interstitial fluid as indicated by the removal of extracellular markers from rat caudate nucleus. Exp Eye Res 1977;25(suppl):461–473.
17 Ichimura T, Fraser PA, Cserr HF: Distribution of extracellular tracers in perivascular spaces of the rat brain. Brain Res 1991;545:103–113.
18 Ohata K, Marmarou A, Povlishock JT: An immunocytochemical study of protein clearance in brain infusion edema. Acta Neuropathol (Berl) 1990;81:162–177.
19 Bradley WG Jr, Scalzo D, Queralt J, Nitz WN, Atkinson DJ, Wong P: Normal-pressure hydrocephalus: evaluation with cerebrospinal fluid flow measurements at MR imaging. Radiology 1996;198:523–529.
20 Stoquart-ElSankari S, Baledent O, Gondry-Jouet C, Makki M, Godefroy O, Meyer ME: Aging effects on cerebral blood and cerebrospinal fluid flows. J Cereb Blood Flow Metab 2007;27:1563–1572.
21 Del Bigio M: Neuropathological changes caused in hydrocephalus. Acta Neuropathol 1993;85:573–585.
22 Biot M: Theory of elasticity and consolidation for a porous anisotropic solid. J Appl Phys 1955;26:182–185.
23 Foss T, Eide PK, Finset A: Intracranial pressure parameters in idiopathic normal pressure hydrocephalus patients with or without improvement of cognitive function after shunt treatment. Dement Geriatr Cogn Disord 2007;23:47–54.

24 Levine DN: The pathogenesis of normal pressure hydrocephalus: a theoretical analysis. Bull Math Biol 1999;61:875–916.
25 Gjerris F, Borgesen S: Pathophysiology of cerebrospinal fluid circulation; in Crockard A, Hayward R, Hoff J (eds): Neurosurgery: The Scientific Basis of Clinical Practice. Oxford, Blackwell Science, 2000, pp 147–168.
26 Bering EA Jr: Circulation of the cerebrospinal fluid. Demonstration of the choroid plexuses as the generator of the force for flow of fluid and ventricular enlargement. J Neurosurg 1962;19:405–413.
27 Wilson CB, Bertan V: Interruption of the anterior choroidal artery in experimental hydrocephalus. Arch Neurol 1967;17:614–619.
28 McCracken PJ, Manduca A, Felmlee J, Ehman RL: Mechanical transient-based magnetic resonance elastography. Magn Reson Med 2005;53:628–639.
29 Czosnyka ZH, Cieslicki K, Czosnyka M, Pickard JD: Hydrocephalus shunts and waves of intracranial pressure. Med Biol Eng Comput 2005;43:71–77.
30 Czosnyka Z, Czosnyka M, Richards HK, Pickard JD: Laboratory testing of hydrocephalus shunts – conclusion of the U.K. Shunt Evaluation Programme. Acta Neurochir (Wien) 2002;144:525–538.
31 Kadowaki C, Hara M, Numoto M, Takeuchi K: Factors affecting cerebrospinal fluid flow in a shunt. Br J Neurosurg 1987;1:467–475.
32 Drake JM, Kestle JR, Milner R, Cinalli G, Boop F, Piatt J Jr, Haines S, Schiff SJ, Cochrane DD, Steinbok P, MacNeil N: Randomized trial of cerebrospinal fluid shunt valve design in pediatric hydrocephalus. Neurosurgery 1998;43:294–305.
33 Hakim S: Hydraulic and mechanical mismatching of valve shunts used in the treatment of hydrocephalus: the need for a servovalve shunt. Dev Med Child Neurol 1973;15:646–653.
34 Zagzoule M, Marc-Vergnes JP: A global mathematical model of the cerebral circulation in man. J Biomech 1986;19:1015–1022.
35 Gjerris F, Borgensen SE: Pathophysiology of Cerebrospinal Fluid Circulation. Cambridge, Blackwell Scientific, 1992.
36 Fishman R: Cerebrospinal Fluid in Disease of the Nervous System. Philadelphia, Saunders, 1980.
37 Wilcox RK, Bilston LE, Barton DC, Hall RM: Mathematical model for the viscoelastic properties of dura mater. J Orthop Sci 2003;8:432–434.
38 Bertram CD, Brodbelt AR, Stoodley MA: The origins of syringomyelia: numerical models of fluid/structure interactions in the spinal cord. J Biomech Eng 2005;127:1099–1109.
39 Smillie A, Sobey I, Molnar Z: A hydroelastic model of hydrocephalus. J Fluid Mech 2005;539:417–433.
40 Kaczmarek M, Subramaniam RP, Neff SR: The hydromechanics of hydrocephalus: steady-state solutions for cylindrical geometry. Bull Math Biol 1997;59:295–323.